Bioactive Materials 6 (2021) 3485–3495

Contents lists available at ScienceDirect

Bioactive Materials

journal homepage: www.sciencedirect.com/journal/bioactive-materials

Hypoxia-mimicking 3D bioglass-nanoclay scaffolds promote endogenous bone regeneration

Xiao Zheng [a], Xiaorong Zhang [b,c], Yingting Wang [c], Yangxi Liu [d,e], Yining Pan [a], Yijia Li [a], Man Ji [a], Xueqin Zhao [f], Shengbin Huang [c,g,**], Qingqing Yao [a,*]

[a] Institute of Advanced Materials for Nano-Bio Applications, School of Ophthalmology & Optometry, Eye Hospital, Wenzhou Medical University, 270 Xueyuan Xi Road, Wenzhou, Zhejiang, 325027, PR China
[b] Department of Endodontics, School and Hospital of Stomatology, Wenzhou Medical University, Wenzhou, PR China
[c] Institute of Stomatology, School and Hospital of Stomatology, Wenzhou Medical University, Wenzhou, PR China
[d] Comprehensive Transplant Center, Feinberg School of Medicine, Northwestern University, USA
[e] Department of Surgery, Feinberg School of Medicine, Northwestern University, USA
[f] College of Life Science and Medicine, Zhejiang Sci-Tech University, Hangzhou, 310018, PR China
[g] Department of Prosthodontics, School and Hospital of Stomatology, Wenzhou Medical University, Wenzhou, China

ARTICLE INFO

Keywords:
3D bioglass scaffold
Hypoxia
Angiogenesis
Osteogenesis
Endogenous bone regeneration

ABSTRACT

Large bone defect repair requires biomaterials that promote angiogenesis and osteogenesis. In present work, a nanoclay (Laponite, XLS)-functionalized 3D bioglass (BG) scaffold with hypoxia mimicking property was prepared by foam replication coupled with UV photopolymerization methods. Our data revealed that the incorporation of XLS can significantly promote the mechanical property of the scaffold and the osteogenic differentiation of human adipose mesenchymal stem cells (ADSCs) compared to the properties of the neat BG scaffold. Desferoxamine, a hypoxia mimicking agent, encourages bone regeneration via activating hypoxia-inducible factor-1 alpha (HIF-1α)-mediated angiogenesis. GelMA-DFO immobilization onto BG-XLS scaffold achieved sustained DFO release and inhibited DFO degradation. Furthermore, *in vitro* data demonstrated increased HIF-1α and vascular endothelial growth factor (VEGF) expressions on human adipose mesenchymal stem cells (ADSCs). Moreover, BG-XLS/GelMA-DFO scaffolds also significantly promoted the osteogenic differentiation of ADSCs. Most importantly, our *in vivo* data indicated BG-XLS/GelMA-DFO scaffolds strongly increased bone healing in a critical-sized mouse cranial bone defect model. Therefore, we developed a novel BG-XLS/GelMA-DFO scaffold which can not only induce the expression of VEGF, but also promote osteogenic differentiation of ADSCs to promote endogenous bone regeneration.

1. Introduction

Natural bone healing is a well-orchestrated process that involves multiple physiological events, including acute inflammation, recruitment of mesenchymal stem cells (MSCs) to generate a primary cartilaginous callus, revascularization and calcification, and bone remodeling [1–4]. Despite the self-healing capacity of bone tissue, delayed union or non-union formations were caused by tumor resection, trauma, infection, and skeletal abnormalities [5–7]. Among all these processes, angiogenesis plays a crucial role in bone regeneration because the bone is a highly vascularized tissue. Neovascularization not only provides necessary nutrition and microenvironments for new bone formation, but also allows for the inflammatory cells, cartilage cells and bone progenitor cells to reach the injury site [8,9]. Moreover, angiogenesis and osteogenesis have a reciprocal relationship during bone remodeling [10–12]. Hence, it is of great importance to develop multi-functional biomaterials with the appropriate mechanical, antibacterial, osteoconductive, osteoinductive and angiogenic properties in bone regeneration [13–15]. Our previous work reported that deferoxamine (DFO), an iron chelator and hypoxia mimicking agent, increased

Peer review under responsibility of KeAi Communications Co., Ltd.
* Corresponding author.
** Corresponding author. Institute of Advanced Materials for Nano-Bio Applications, School of Ophthalmology & Optometry, Eye Hospital, Wenzhou Medical University, Wenzhou, PR China.
E-mail addresses: huangsb003@wmu.edu.cn (S. Huang), qingqingyao@wmu.edu.cn (Q. Yao).

https://doi.org/10.1016/j.bioactmat.2021.03.011
Received 3 October 2020; Received in revised form 8 February 2021; Accepted 3 March 2021

vascular endothelial growth factor (VEGF) expressions in both human mesenchymal stem cells (hMSCs) and human umbilical vein endothelial cells (HUVEC), thus activated endogenous hypoxia mediated-angiogenesis and promoted new bone formation [16]. However, *in vitro* cell experiments showed that the DFO-loaded gelatin nanofibrous scaffolds inhibited the osteogenic differentiation of hMSCs. Additional osteogenic signals were still required in order to promote osteogenic differentiation during bone healing process.

45S5 Bioglass (BG) is composed of 45% SiO_2, 24.5% Na_2O, 24.5% CaO, and 6% P_2O_5 and has good bioactivity, osteoconductivity and bonding ability to living bone tissue [17–19]. However, 3D BG scaffolds in bone tissue engineering are often impeded by its brittleness, low fracture toughness and poor osteoinductivity [20]. Doping other metal ions or polymer into the silicon-based network is an effective way to increase the mechanical properties of BG scaffolds [21–25]. For example, Cao et al. has dopped ZnO and MgO into the 45S5 BG scaffolds to demonstrated enhanced compressive strength and fracture toughness after doping [26]. It has been reported that the 2D Nanosilicate (Laponite®, XLS), a magnesium silicate ($Na^{+}_{0.7}[(Si_8Mg_{5.5}Li_{0.3})O_{20}(OH)_4]^{-}_{0.7}$), can significantly enhance the mechanical properties of polymeric matrix because XLS nanosheet can act as the filler and physical crosslinker to the polymer [27–29]. Moreover, studies have demonstrated that XLS can also facilitate the cells' adhesion, proliferation, and osteogenic differentiation [27,29–32]. Wang et al. prepared 3D XLS scaffold by sintering and the scaffold maintained the ability to enhance the osteogenic differentiation of hMSCs without adding any exogenous growth factors [33]. In this work, we developed a dual-functional 45S5 BG scaffolds with both angiogenic and osteogenic properties to promote bone tissue regeneration. The incorporation of XLS into BG scaffolds improved its mechanical property and osteoblastic differentiation ability. The immobilization of GelMA-DFO onto the BG scaffolds prolongs the release duration of DFO over 21 days and promotes VEGF expression in ADSCs. Moreover, *in vivo* data suggested that the prepared BG-XLS/GelMA-DFO scaffolds can significantly promote bone formation in a critical-size cranial bone defect model.

2. Materials and methods

2.1. Materials

45S5 Bioglass was purchased from (Dingan Tec, China). Polycaprolactone (Mn = 80000) and Gelatin type A (from porcine skin) were purchased from Sigma (St. Louis MO, USA). Desferoxamine was purchased from Abcam (MA, USA). XLS nanoparticles were purchased from Nanocor (Beijing, China). Iron (III) chloride($FeCl_3$), Methacrylic anhydride (MA) and dimethyl carbonate (DMC) were purchased from MACKLIN (Shanghai, China). Omnirad 2959 photoinitiators was purchased from YANGFAN NEW MATERIALS (Zhejiang, China). ADSCs were purchased from Cyagen (Shanghai, China).

2.2. Preparation of BG and BG-XLS scaffolds

BG scaffolds were prepared by a foam replication method as previously described [34]. Briefly, PCL was dissolved in dimethyl carbonate solution and 40 wt% 45S5 Bioglass powder (~2 μm) was then added into the prepared PCL solution. Afterwards, polyurethane (PU) was immersed in the PCL/Bioglass slurry and squeezed out the excess slurry and dried at 60 °C. We repeated the above steps three times and sintered the green bodies at 1000 °C to obtain BG scaffolds.

For preparation of BG-XLS scaffolds, different concentrations of XLS (1 wt%, 3 wt%, 5 wt%) (BG-XLS1, BG-XLS3, BG-XLS5)were added into the PCL/Bioglass slurry to prepare a homogeneous PCL/Bioglass-XLS slurry. The same procedure was used as to prepare BG scaffolds.

2.3. Preparation of BG-XLS/GelMA-DFO scaffolds

To prepare gelatin methacrylamide (GelMA), 10 g of gelatin A was dissolved in 37 °C DPBS solution and stirred for 1 h to get a homogeneous solution. MA was then added into the prepared gelatin solution and stirred for 3 h at 50 °C. The mixed solution was then dialyzed in DI water for one week and DI water was changed twice daily. Lastly, the samples were freeze dried for 24 h.

To prepare DFO loaded BG-XLS scaffolds, GelMA was first dissolved at pure water at 40 °C. Omnirad 2959 photo-initiators and DFO were added into the GelMA solution to make a homogeneous solution. 100 μL GelMA-DFO solution that contained 100 μmol of DFO was then dropped onto the prepared BG-XLS scaffolds and exposed to the UV light at 365 nm and crosslinked for 10 min to acquire the BG-XLS/GelMA-DFO scaffolds.

2.4. Physicochemical characterization of BG, BG-XLS and BG-XLS/GelMA-DFO scaffolds

The morphologies of scaffolds were studied by using a scanning electron microscope (FEI, USA). The prepared scaffolds were sputter-coated for 45 s and observed at an accelerating potential of 15 kV. The compressive properties of BG, BG-XLS1, BG-XLS3 and BG-XLS5 scaffolds were measured by a universal testing machine with the crosshead speed of 1 mm/min.

2.5. In vitro bioactivity of scaffolds

The biomimetic mineralization property is a marker of the bioactive behavior of biomaterials, BG, BG-XLS1 and BG-XLS3 scaffolds were immersed in 10 mL of Kokubo's simulated body fluid (SBF) and incubated at 37 °C and shaken at 90 rpm [35]. After 1 and 4 days of immersion, the scaffolds were collected and washed with DI water to remove the additional SBF solution and the scaffolds were frozen at −20 °C and then freeze dried.

2.6. In vitro degradation

BG-XLS and BG-XLS/GelMA scaffolds were used in the *in vitro* degradation study. Weighed samples were placed in clean glass vials containing 10 mL PBS solution and incubated at 37 °C. The PBS solution was replaced every two days, and after each soaking time, samples were collected and washed with distilled water and dried at 60 °C. Weight loss was calculated by Eq. (1), where W_0 is the initial mass and W_1 is the mass after PBS immersion.

$$\text{Weight loss } (\%) = [(W_0 - W_1)/W_0] \times 100 \quad (1)$$

2.7. In vitro DFO release

BG-XLS/GelMA-DFO and BG-XLS-DFO scaffolds were used in the *in vitro* drug release study. Each scaffold was immersed in 2 mL of pure water and placed in a incubator at 37 °C and shaken at 90 rpm in a vial. At each time point, 1 mL of supernatant was collected and 1 mL of fresh pure water was added back into the vial. After 21 days of released, DFO amount was determined as previously described [16]. Briefly, 100 μL of the collected solution was reacted with same volume of 3 mM of $FeCl_3$ solution for 10 min. The concentration of DFO was measured by a UV spectrophotometer at 485 nm.

2.8. Enzyme linked immunosorbent assay (ELISA)

ADSCs were seeded onto 24 well plate, and cultured overnight. DFO (20 μM) contained culture medium and scaffold extracts (BG-XLS/DFO,

BG-XLS/GelMA-DFO) were applied to the ADSCs. After each incubation time, supernatant was collected and the amount of VEGF was quantified by a human VEGF ELISA Development Kit (Peprotech, Rocky Hill, NJ, USA). VEGF expression was measured by a microplate reader (Spectramax M5, Molecular Devices, USA) at 405 nm. The amount of hypoxia-inducible factor-1 alpha (HIF-1α) was calculated by a human HIF-1α ELISA Kit (WESTANG BIO-TECH, Shanghai, China). The sample's absorbance at 450 nm was measured. Cells without DFO were used as negative control.

2.9. In vitro cell tests

2.9.1. Cell viabilities

Cell viability of MC3T3-E1 cells on BG, BG-XLS1 and BG-XLS3 scaffolds were quantitatively analyzed using CCK8 assay. Briefly, 2×10^4 MC3T3-E1cells were seeded onto BG, BG-XLS1 and BG-XLS3 scaffolds. After each culture time, culture medium was removed and culture medium with 10% CCK8 was added and incubated for another 1 h at 37 °C. The absorbance at 450 nm was measured by using the microplate reader. BG scaffold group was used as the control group.

To study the cell morphology on BG, BG-XLS1 and BG-XLS3 scaffolds, 2×10^4 MC3T3-E1 cells were seeded onto the scaffolds and culture for 1 and 4 days. Afterwards, culture medium was removed and the scaffold was washed with DPBS solution twice and then fixed in 2.5% glutaraldehyde solution at 4 °C for 3 h. The sample was dehydrated in 30%, 50%, 70%, 90% and 100% ethanol solutions for 15 min, respectively. Finally, scaffold was treated with tert-butyl alcohol at 4 °C and freeze-dried, the morphology of the cells was observed by SEM (Prox, Phenom).

2.9.2. Preparation of scaffolds extracts

For the preparation of scaffold extracts, 10 mg of sample (BG, BG-XLS1, and BG-XLS3 scaffold) was immersed into 1 mL culture medium and incubated for 24 h at 37 °C and 5% CO_2. After immersion, the extracts were collected and used for the cell culture.

2.9.3. Osteogenic differentiation of ADSCs on scaffolds

Alkaline phosphatase (ALP) activity of ADSCs on scaffolds was studied as we previously described [36]. Briefly, ADSCs (5×10^4) seeded onto a 24 well plate and cultured overnight. Next, scaffold extracts were added and cultured for 7 days. ALP activity was measured by an ALP assay kit according to the manufacturer's instruction and normalized against total protein content. The total protein content was measurement by a bicinchoninic acid (BCA) kit.

Biomineralization of ADSCs on scaffolds was also investigated. ADSCs were seeded onto the scaffolds and cultured for 21 days. Then, culture medium was removed and the cells/scaffold was washed with DPBS twice. Then 1 mL of 6 M hydrochloric acid was added into the cells/scaffold to extract calcium, and the calcium concentration was quantified by using a total calcium LiquiColor® kit (Stanbio laboratory, TX).

To further study the influence of the prepared scaffolds on the osteogenesis of ADSCs, osteogenesis related genes (RUNX2 and OCN) were also investigated. As we previously described [36], we extracted the total RNA by using the GeneJET™ RNA Purification Kit, and an equivalent amount of RNA was processed to generate cDNA using the High Capacity cDNA Reverse Transcript kit. Quantitative PCR was carried out with Taqman gene expression assays. Gene primers of GAPDH (Mm99999915), RUNX2 (Mm00501584) and OCN (Mm03413826) were purchased from Applied Biosystems (Förster City, USA).

2.10. In vivo cranial bone regeneration

5–6 weeks old Sprague Dawlye (SD) male rats were used to create critical-sized cranial bone defect model for *in vivo* study. Care, housing and surgery procedure use of laboratory animals followed the protocol approved by the Animal Ethics Committee of Wenzhou Medical University (China). An 8 mm defect was made and sterilized BG-XLS, BG-XLS/GelMA-DFO and BG-XLS-BMP2 scaffolds were implanted into the cranial defects. 1 mg/mL of bone morphogenetic protein-2 (BMP2) (Peprotech, Rocky Hill, NJ, USA) solution was mixed with collagen solution (2.5 mg/mL, Bedford, MA, USA), and 1 M NaOH solution was used to adjust the pH value to 7.4. Finally, 10 μL of the collagen/BMP2 solution with 1 μg BMP2 was then incorporated into the BG-XLS scaffolds. The BG-XLS-BMP2 group was chosen as the positive control. All SD rats were euthanized after 8 weeks of implantation, followed by being fixed with 10% formalin for 2 days, then immersed in 70% ethanol for radiographic (Bruker, Billerica, MA, USA) and micro-CT (Skyscan 1076, Bruker, USA) analysis. After the μCT analysis, the decalcification process of samples was carried out in a 10% EDTA (pH = 7.4) solution for 3 weeks and the samples were then imbedded in paraffin for histological analysis. The tissue slices were cut with the thickness of 5 μm and stained with Hematoxylin and Eosin (H&E) and observed under microscope (IX 2-UCB, Olympus).

3. Results and discussion

3.1. ALP staining of sintered XLS and BG scaffolds on ADSCs

Our previous study reported that the XLS can facilitate the osteogenic differentiation of hMSCs. However, the influences of BG scaffolds and sintered XLS on the osteogenesis of ADSCs have not been investigated. Here, BG scaffold extracts and sintered XLS extracts were used for ALP study. ALP staining data exhibited sintered XLS extracts significantly increased ALP expression compared to BG scaffold extracts in ADSCs after 7 days of culture (Fig. 1 (left panel)). Similarly, the quantification data of ALP activities also showed that sintered XLS extracts had more positive effects on the osteogenic differentiation of ADSCs than BG scaffold extracts (Fig. 1 (right panel)). Therefore, it is an effective strategy to incorporate XLS into BG scaffolds to increase osteogenic differentiation ability of ADSCs.

3.2. Characterization of XLS functionalized BG scaffolds

Certain amount of XLS (1 wt%, 3 wt%, 5 wt%) was added into the 45S5 bioglass slurry to prepare 3D BG-XLS scaffolds by foam replication method. SEM images of sintered BG scaffolds with and without XLS incorporation are shown in Fig. 2(a–h). All four types of scaffolds exhibited an interconnected open macroporous structure with the pore size between 100 and 500 μm. Moreover, microporous structure, which increases the surface area of the prepared scaffolds, was also observed. Both macroporous and microporous structure benefit cell attachment, proliferation and blood vessels formation [37,38]. It was noted that the increase of XLS concentration from 0% to 5% led to the decrease of the porosity of scaffolds (95.5% *vs* 71.5%) (Fig. 2(i)), while the shrinkage of scaffolds was dramatically increased (21.5% *vs* 55.1%) compared to original PU foam (Fig. 2(j)). The mechanical properties of BG, BG-XLS1, BG-XLS3 and BG-XLS5 scaffolds are shown in Fig. 2(k). The increase of XLS concentration to 0%, 1%, 3%, 5% led to the compressive modulus to 0.36 MPa, 0.55 MPa, 3.36 MPa and 9.91 MPa, respectively. These results indicated that the incorporation of XLS drastically increased the compressive strength of BG scaffolds. Based on the porosity, pore size, morphology and mechanical data, BG-XLS1 and BG-XLS3 scaffolds were chosen for the ensuing experiments and BG scaffolds were used as control.

SEM images of BG-XLS3 and BG-XLS3/GelMA scaffolds are shown in Fig. 3. After GelMA coating, interconnected open macroporous structure of BG-XLS3 scaffolds was maintained, and the surface became smoother. silicon (Si), sodium (Na), calcium (Ca), phosphate (P), magnesium (Mg) ions were detected from the EDS spectra of BG-XLS3 and BG-XLS3/GelMA scaffolds, where Mg ion was from XLS. No lithium (Li) ion was detected from the EDS spectra of BG-XLS3, which may be due to the

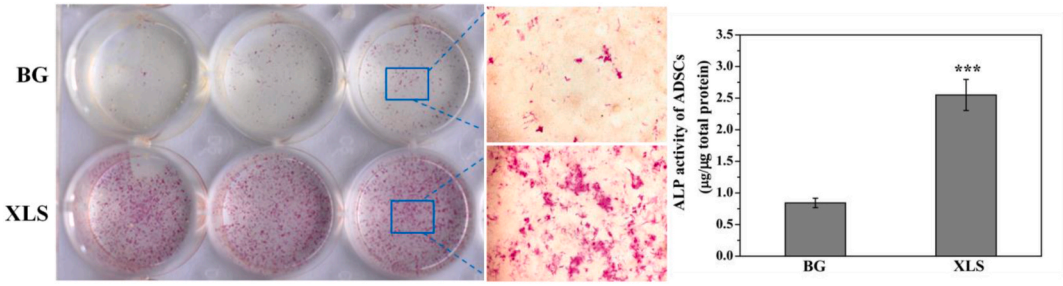

Fig. 1. ALP staining of ADSCs after treated with BG extracts and sintered XLS extracts (left panel), ALP activities of ADSCs after treated with BG extracts and sintered XLS extracts (right panel).

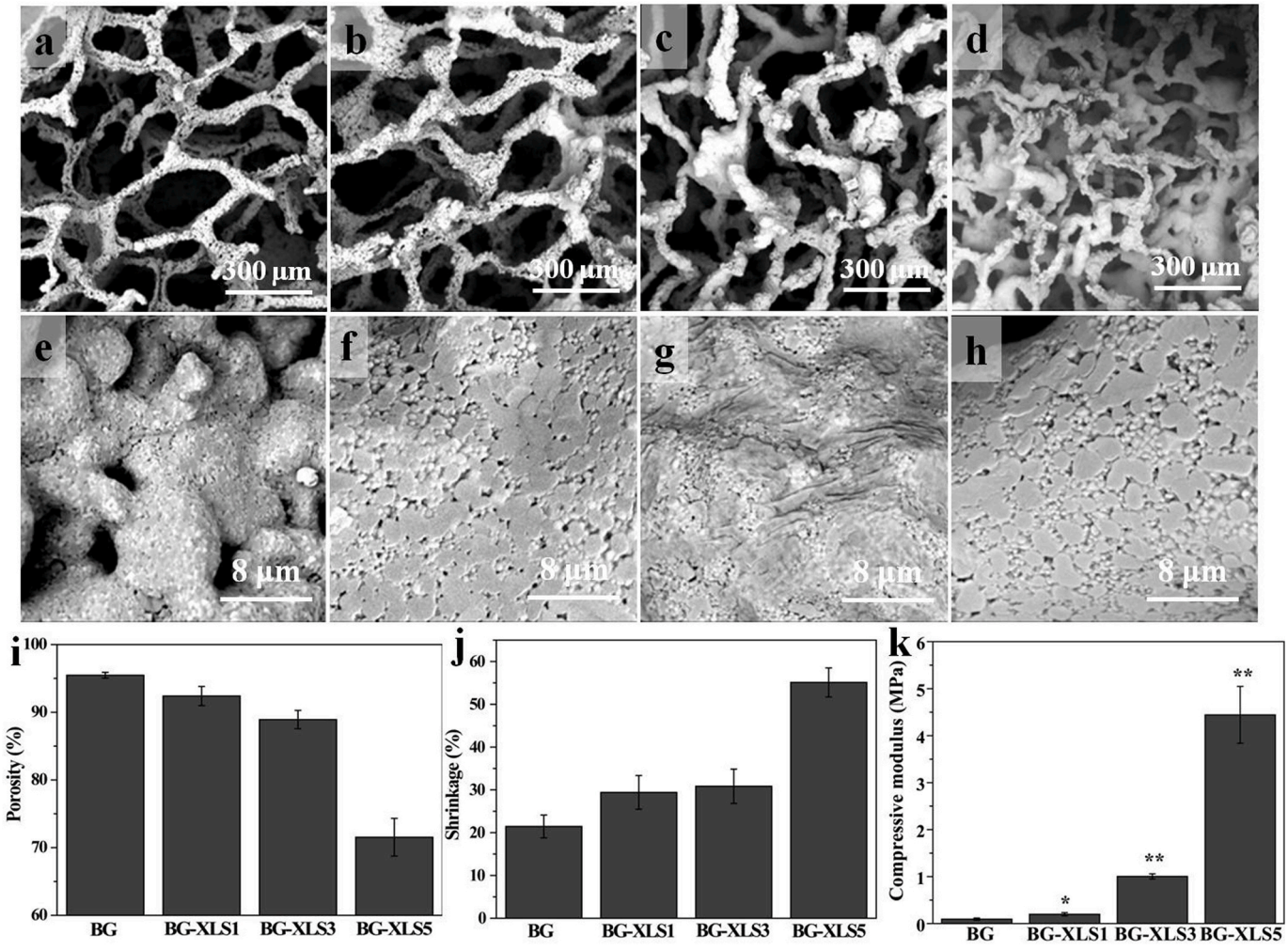

Fig. 2. SEM images of (a, e) BG scaffold, (b, f) BG-XLS1 scaffold, (c, g) BG-XLS3 scaffold, (d, h) BG-XLS5 scaffold; (i, j) Porosity and shrinkage of BG, BG-XLS1, BG-XLS3 and BG-XLS5 scaffolds, respectively; (k) Compressive strength of BG, BG-XLS1, BG-XLS3 and BG-XLS5 scaffolds. Data are expressed as mean ± SD ($n = 3$). (*$P <$ 0.05, **$P < 0.05$).

content of Li ion was very low in the XLS (0.8 wt%). The mechanical properties of BG-XLS3 and BG-XLS3/GelMA scaffolds are shown in Fig. 3 (g). The BG-XLS3/GelMA scaffold showed higher compressive modulus than BG-XLS3 scaffold, while no significant difference was observed between two scaffolds. The *in vitro* degradation behaviors of BG-XLS and BG-XLS/GelMA scaffolds showed that GelMA was mainly dissolved within the first 24 h and the degradation behaviors were similar between BG-XLS3 and BG-XLS3/GelMA scaffolds in a period of 14 days.

3.3. *In vitro* bioactivity of scaffolds

In vitro biomineralization study is an effective way to assess the bioactivity of biomaterials. Our previous study showed good *in vitro* bioactivity of BG scaffolds [20], while the bioactivity of BG scaffolds after XLS incorporation was not studied. After 1 day of immersion in SBF, all three types of scaffolds were covered with hydroxyapatite (HA), and had a Ca to P ratio around 1.5. Afterwards, we measured the FTIR and XRD spectra of BG-XLS3 and BG-XLS3 scaffolds after immersed in SBF for 1 day (Fig. 4 (j, k)). The FTIR spectra showed that characteristic

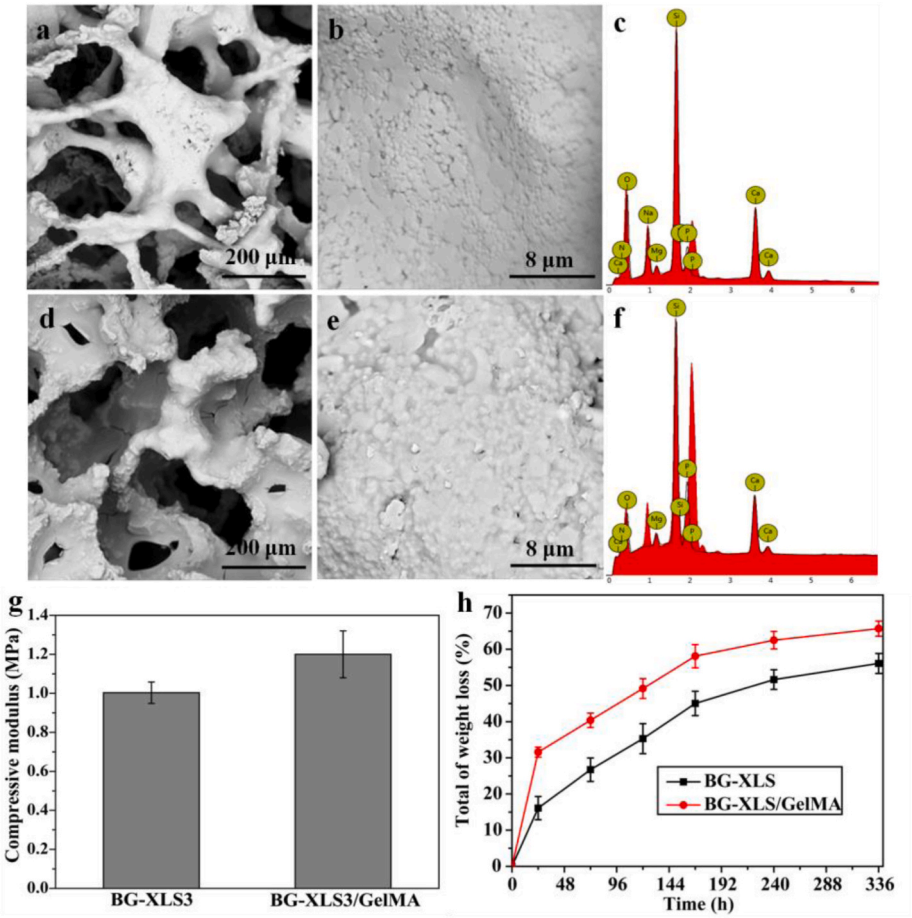

Fig. 3. SEM images (a, b) BG-XLS3 and (d, e) BG-XLS3/GelMA; EDS spectra of (c) BG-XLS3 and (f) BG-XLS3/GelMA scaffolds; (g) Compressive strength of BG-XLS3 and BG-XLS3/GelMA scaffolds; (h) *In vitro* weight loss of BG-XLS and BG-XLS/GelMA scaffolds after immersion in PBS solution for 14 days.

peaks of HA were observed at 564 and 603 cm^{-1}, which were attributed to the $PO4^{3-}$. In addition, the characteristic peak at 877 cm^{-1} was belonged to the bending vibrations of C–O bond. XRD spectra also exhibited characteristic peak of HA at around 32°. All these data indicated that the incorporation of XLS onto BG scaffold had no effect on its bioactive property to form carbonated hydroxyapatite (HCA). The HCA layer can form a rapid, strong bond between bioglass and bone tissue to improve osseointegration [40].

3.4. *In vitro cell studies*

MC3T3-E1 cells viability on BG, BG-XLS1 and BG-XLS3 scaffolds were quantitatively measured by CCK8 assay after 1 and 4 days of culture. On day 1, the BG-XLS3 group showed higher cell viability compared to BG and BG-XLS1 groups. While on day 4, all groups exhibited similar cell viabilities. Additionally, cell morphologies on all three types of scaffolds were also investigated. As shown in Fig. 5(b–d), after 1 day of culture, cells were fully attached and elongated on all three types of scaffolds. On day 4, cells proliferated and presented polygonal morphologies and no obvious morphology differences were observed on all three types of scaffolds Fig. 5 (e-g). The incorporation of XLS into BG scaffolds had little impact on the viabilities and morphologies of MC3T3-E1 cells.

To study the effect of scaffolds on cellular mineralization, ADSCs were cultured on the three types of scaffolds extracts. After 21 days of culture, alizarin red stained calcium nodules were found on all samples and significantly more positive mineral nodules were observed on XLS contained scaffolds compared to BG scaffolds. Consistent with the qualitative staining data, quantitative data exhibited neat BG scaffolds significantly promoted the mineralization of ADSCs compared to that of control group (Fig. 6 right panel) (**$P < 0.01$), and highest amount of calcium was detected on BG-XLS3 scaffolds. BG scaffold alone has the ability to promote the mineralization of ADSCs and a synergistic effect with XLS was observed when the XLS concentration was increased to 3 wt%.

Previously, ALP data (Fig. 1) showed BG scaffolds extract was not able to largely promote the ALP activity of ADSCs. However, our biomeralization data exhibited a stronger promoting effect of BG scaffolds extracts on the ADSCs mineralization. These may be due to the 45S5 bioglass which is composed of 45% SiO_2, 24.5% Na_2O, 24.5% CaO, and 6% P_2O_5, and the dissolution from 45S5 bioglass such as Ca, P and Si were favorable to extracellular matrix mineralization, calcification of bone tissue and increases bone mineral density [42,43]. XLS ($Na^{+}_{0.7}[(Si_8Mg_{5.5}Li_{0.3})O_{20}(OH)_4]^{-}_{0.7}$) is a disk-shaped crystal with a diameter around 25 nm and a height around 1 nm [27]. The dissolution products of XLS, such as Li and Mg ions can promote the osteogenic differentiation of stem cells [21,40]. For example, Zhang et al. [45] reported that Li can activate Wnt/β-catenin signaling through inhibition of glycogen synthetase kinase-3β (GSK-3β) and then the activated Wnt/β-catenin signaling pathway can enhance the osteogenesis of stem cells.

3.5. *5. In vitro DFO release*

BG-XLS with physically absorbed DFO (BG-XLS-DFO) and BG-XLS/GelMA-DFO scaffolds were used for the *in vitro* DFO release study. The release profiles of DFO from BG-XLS-DFO and BG-XLS/GelMA-DFO scaffolds are shown in Fig. 7. An initial burst release was achieved in

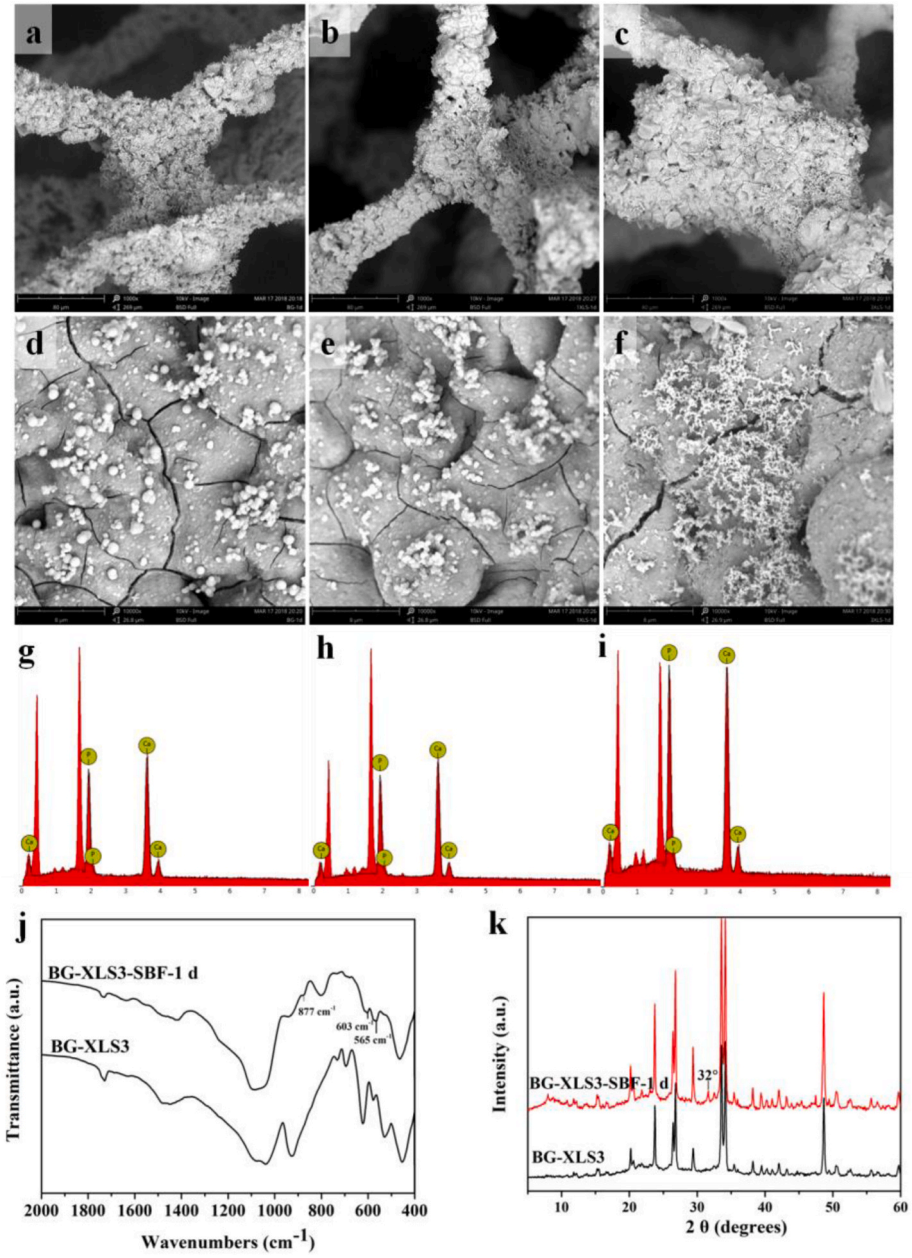

Fig. 4. SEM images and EDS spectra of (a, d, g) BG scaffolds, (b, e, h) BG-XLS1 scaffolds and (c, f, i) BG-XLS3 scaffolds after 1 d of SBF immersion; (j) FTIR spectra and (k) XRD spectra of BG-XLS3 scaffolds and BG-XLS3 scaffolds after immersed in SBF for 1 d.

the first 12 h followed by a period of sustained release for 21 days. It is interesting to note that though similar release profiles were observed on two scaffolds, significantly higher percentage of DFO was released from the BG-XLS/GeLMA-DFO scaffolds compared to BG-XLS-DFO scaffolds in a period of 21 days. These data indicated that macroporous and microporous structure of 3D BG scaffolds contributed to the long-term sustained release of DFO and the photo-crosslinking of GelMA-DFO protected the degradation of DFO.

3.6. HIF-1α and VEGF expression in ADSCs

HIF-1α and VEGF expressions on neat DFO solution (100 μM), BG-XLS scaffolds and BG-XLS/GelMA-DFO (100 μM) scaffolds are shown in Fig. 8. After 24 h of treatment, both DFO and BG-XLS/GelMA-DFO groups elevated the HIF-1α and VEGF expression in ADSCs compared to control, while BG-XLS scaffold did not influence the HIF-1α and VEGF expression in ADSCs. Moreover, after 48 h of culture, BG-XLS/GelMA-DFO group still retained the ability to promote the HIF-1α and VEGF expression, while higher expression levels than the neat DFO group. However, BG-XLS group also elevated the HIF-1α expression in ADSCs at 48 h. It was worth to note that no obvious difference was observed between BG-XLS and BG-XLS/GelMA groups (data not shown), indicating that BG-XLS might have positive effect on HIF-1α expressions in ADSCs and GelMA had no such effect. All these data suggested that the immobilization of DFO onto BG-XLS scaffolds could elongate the release of DFO, thus promoting DFO-induced HIF-1α and VEGF expressions in ADSCs for a longer period.

3.7. In vitro cell viabilities

The cytotoxicity of neat DFO, BG-XLS and BG-XLS/GelMA-DFO scaffolds after 1 and 3 days is shown in Fig. 9. Considerable cell toxicity was found on all DFO, BG-XLS and BG-XLS/GelMA-DFO samples compared to the control group after 1 day of cell culture ($P < 0.05$),

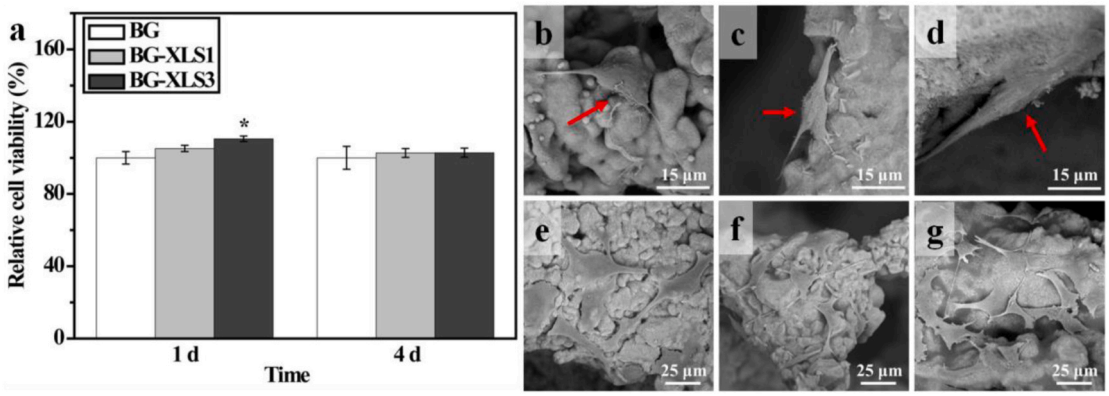

Fig. 5. (a) Relative cell viabilities of MC3T3-E1 cells cultured on BG, BG-XLS1 and BG-XLS3 scaffolds after 1 and 4 days; MC3T3-E1 cells morphologies on (b, e) BG, (c, f) BG-XLS1 and (d, g) BG-XLS3 scaffolds after 1 and 4 days, respectively. Data are expressed as mean ± SD ($n = 3$). (*$P < 0.05$).

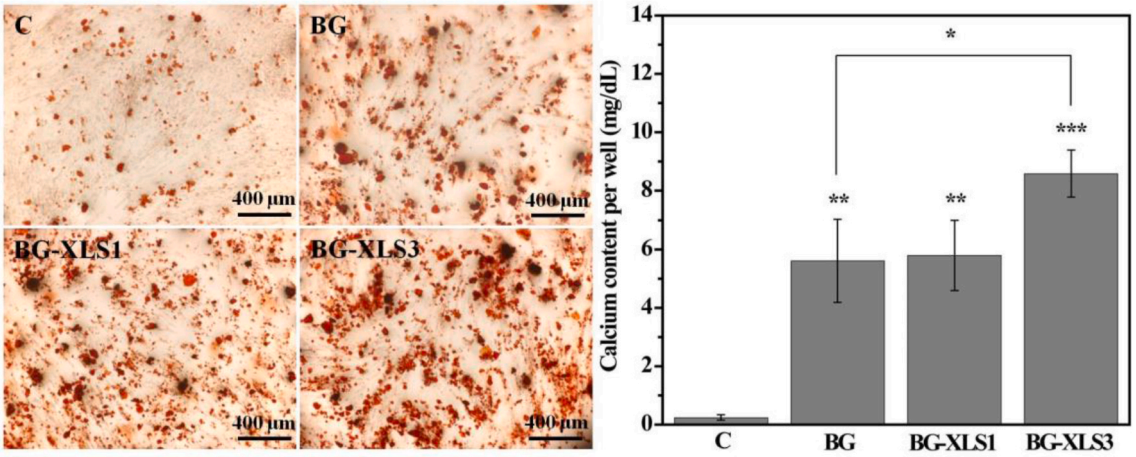

Fig. 6. Effects of BG, BG-XLS1 and BG-XLS3 scaffolds extracts on calcium contents of ADSCs after 21 days of culture. Data are expressed as mean ± SD ($n = 3$). (**$P < 0.01$, ***$P < 0.001$).

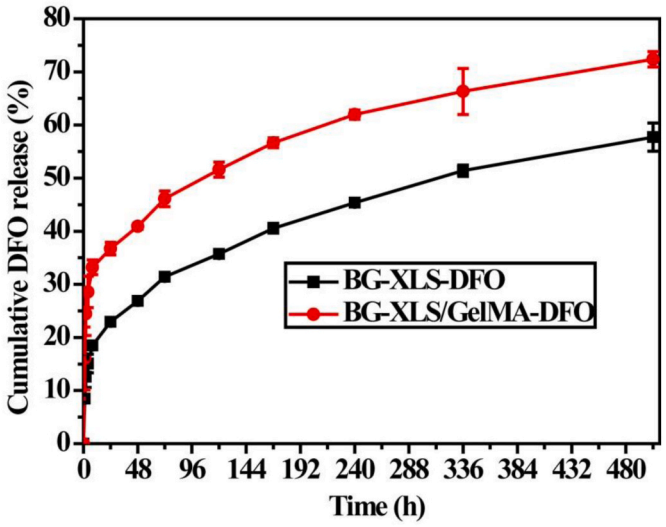

Fig. 7. DFO released from BG-XLS-DFO and BG-XLS/GelMA-DFO scaffolds.

although no obvious differences were observed among the DFO, BG-XLS and BG-XLS/GelMA groups. Moreover, with the incubation time increased to 3 days, the cytotoxicity continued to increase in DFO and BG-XLS/GelMA-DFO groups, while the cell viability on BG-XLS scaffolds showed a slight increase compared to 1 day. The cell viability differences between control and BG-XLS scaffolds on day 1 and day 3 indicated that cells attached and spread slower on the 3D BG-XLS scaffolds compared to 2D tissue culture plate (TCP), but, the cells proliferated quicker afterwards on the 3D BG-XLS scaffolds than 2D TCP. It is worth to mention that on day 3, the BG-XLS/GelMA-DFO scaffolds showed higher cell viability compared to DFO group ($P < 0.05$). This result was consistent with the drug release data that mixed DFO with GelMA and immobilized GelMA-DFO onto the BG-XLS scaffolds that supported a sustained release of DFO and minimized the cytotoxicity of DFO (see Fig. 7).

To study the effects of DFO, BG-XLS and BG-XLS/GelMA-DFO scaffolds on the osteogenic differentiation of ADSCs, ALP activities and biomineralization were investigated (Fig. 10). ALP activity was measured after 7 days of culture, where both BG-XLS and BG-XLS/GelMA-DFO scaffolds significantly promoted the ALP activities of ADSCs compared to control group ($P < 0.01$); no such effect was observed on the DFO group. Furthermore, mineralization data showed higher amount of calcium was detected on DFO, BG-XLS scaffolds and BG-XLS/GelMA-DFO scaffolds compared to that of control. The fold change in neat DFO treated group was not as high as BG-XLS contained scaffold. These data indicated that DFO can only promote the mineralization of ADSCs while BG-XLS scaffolds had positive effects on both ALP activity and mineralization. In addition to ALP activity and calcium content, osteogenic differentiation related gene expressions were also investigated. The ADSCs on BG-XLS/GelMA-DFO scaffolds had

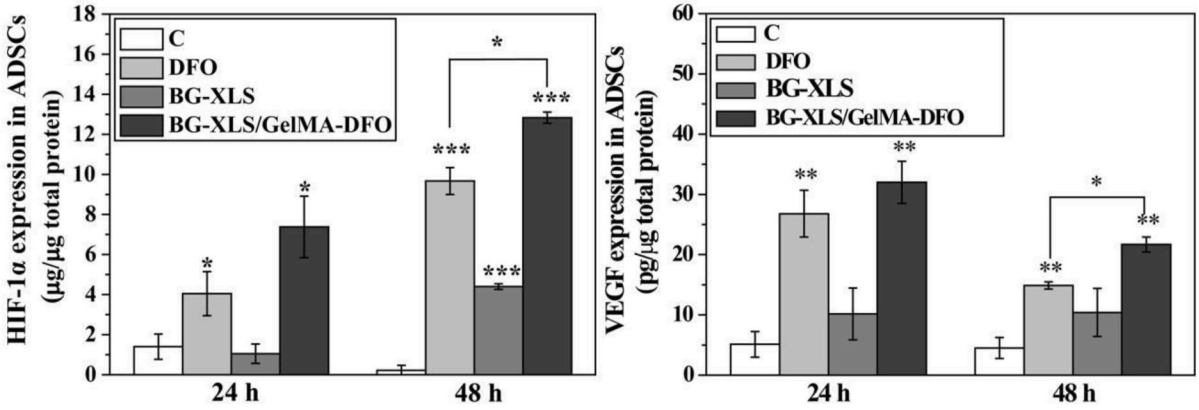

Fig. 8. HIF-1α and VEGF expressions in ADSCs were measured after the cells were cultured in different culture medium for 24 h and 48 h. Data are expressed as mean ± SD ($n = 3$). (*$P < 0.05$, **$P < 0.01$, ***$P < 0.001$).

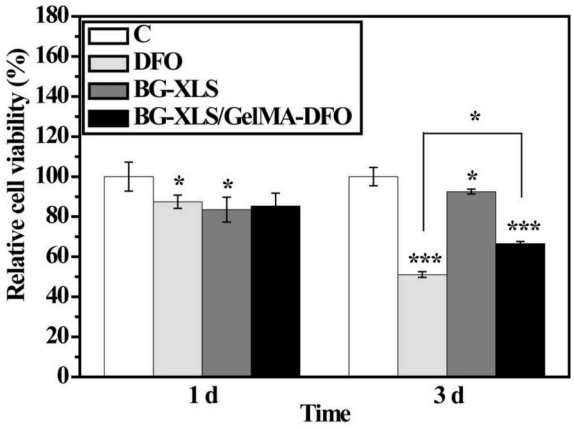

Fig. 9. Relative cell viabilities of ADSCs cultured on control, DFO (100 μM), BG-XLS scaffolds and BG-XLS/GelMA-DFO scaffolds for 1 and 3 days.

significantly higher levels of osteogenic gene expression, including both RUNX2 and OCN (Fig. 11). Our previous study demonstrated that DFO-decorated gelatin nanofibrous scaffolds inhibited the early osteogenic differentiation of hMSCs (ALP activity); however, it promoted mature osteogenic marker OCN, thus, additional osteogenic signals were still required to promote osteogenesis [13,46]. Similar results of DFO-decorated BG scaffolds on the osteogenic differentiation of ADSCs were observed, where DFO is favorable for the biomineralization and OCN expression of ADSCs. Moreover, after the incorporation of XLS into the BG scaffolds, both early and late osteogenic differentiation markers were improved in the BG-XLS/GelMA-DFO scaffold, without using any exogenous growth factors. These results were supported by the previous studies, for example, Gaharwar et al. [47] reported that the XLS was able to act as the osteoinductive agent and promote the ALP activity, RUNX2, OPN and OCN expression of hMSCs in the normal culture media. Xavier et al. [27] prepared GelMA-XLS hydrogel, improved the mechanical property and degradation behavior of hydrogels and the ALP activity and formation of mineralized nodulus of MC3T3-E1 cells were enhanced in normal culture media with the addition of 2 wt% XLS. Our previous study demonstrated that the degradation products of XLS, i.e., SiO_4^{4-}, Mg^{2+} and Li^{+} combined with the strong binding ability of XLS contributed to the improved osteogenic differentiation [49] (see Fig. 11).

3.8. *In vivo* bone regeneration

To further study the influences of the scaffolds on new bone formation *in vivo*, BG-XLS, BG-XLS/GelMA-DFO and BG-XLS-BMP2 (positive control) scaffolds were implanted into a SD rats critical-sized cranial bone defects for 8 weeks. The 3D micro-CT data of the scaffolds revealed that all of three scaffolds showed new bone formation but the BG-XLS/GelMA-DFO and BG-XLS-BMP2 scaffolds had significantly higher new bone volume compared to BG-XLS scaffolds (Fig. 12(a–c)). In addition, our preliminary results showed that no new bone tissue was formed on the BG scaffolds (data not shown). The quantitative data of the bone volume/tissue volume (BV/TV) and bone mineral density (BMD) values were calculated from the 3D micro-CT data (Fig. 12(d and e)). Consistent with the micro-CT data, BG-XLS/GelMA-DFO and BG-XLS-BMP2 scaffolds had higher BV/TV ratio and BMD than BG-XLS scaffolds even though the values of BG-XLS/GelMA-DFO scaffolds were lower than that of BG-XLS-BMP2 scaffolds. Histological staining showed that the interconnected macroporous structures of all three types of scaffolds were

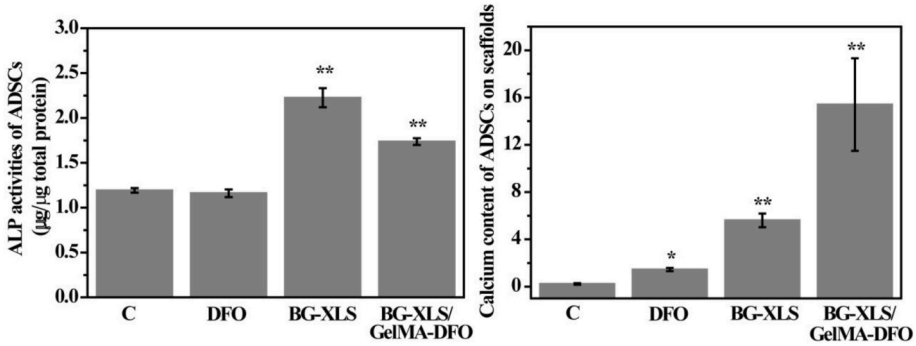

Fig. 10. ALP activity of ADSCs on C, DFO, BG-XLS scaffolds and BG-XLS/GelMA-DFO scaffolds after 7 days of culture. Calcium content of ADSCs on C, DFO, BG-XLS scaffolds and BG-XLS/GelMA-DFO scaffolds after 21 days of culture. *$P < 0.05$, **$P < 0.01$($n = 3$).

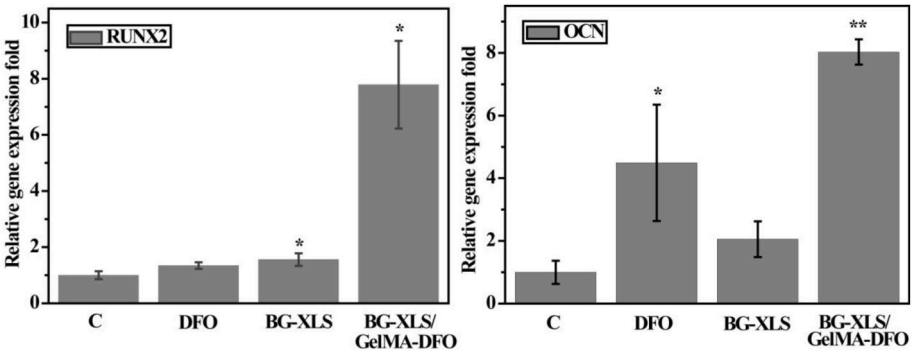

Fig. 11. RUNX2 and OCN expressions after 7 days of culture. *$P < 0.05$, **$P < 0.01$ ($n = 3$).

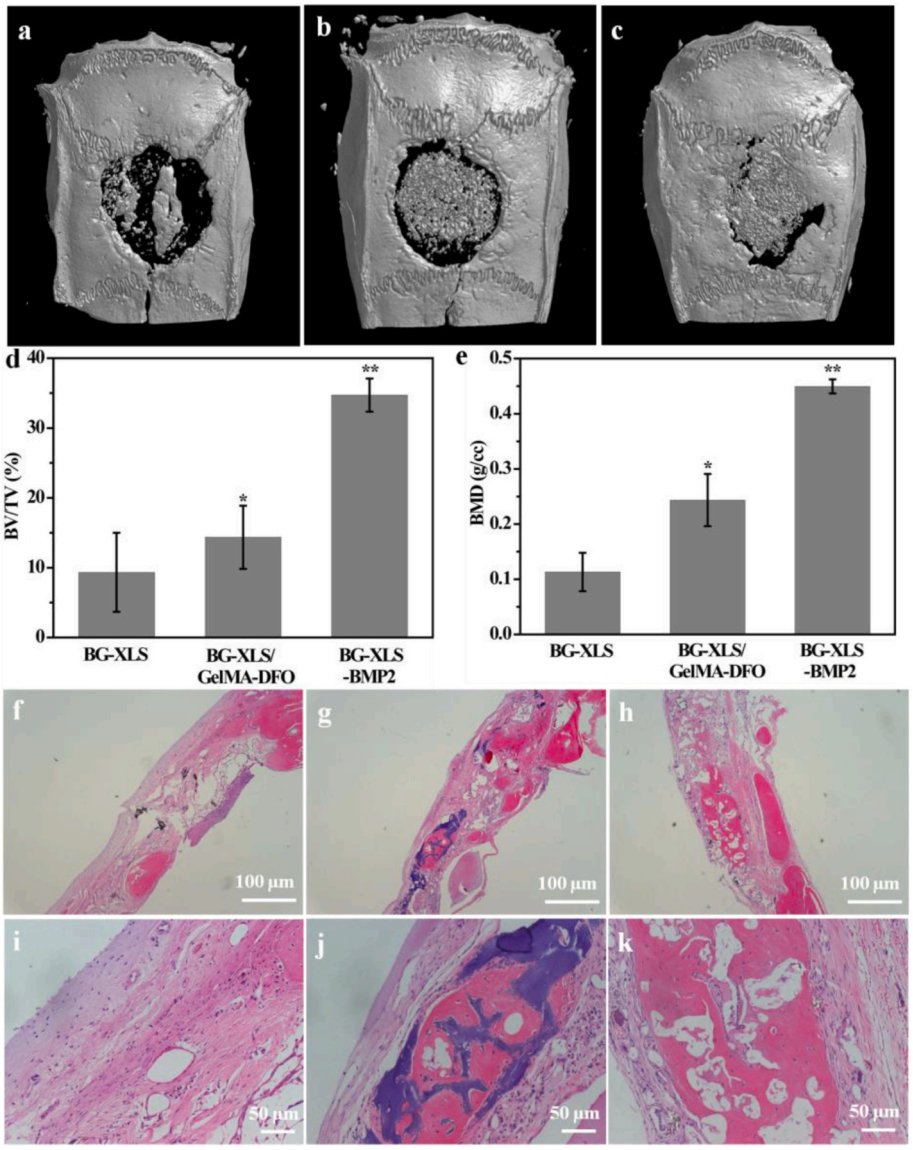

Fig. 12. Micro-CT images of: (a) BG-XLS, (b) BG-XLS/GelMA-DFO, (c) BG-XLS-BMP2 scaffolds at 8 weeks post-operation; (d) BV/TV and (e) BMD values for corresponding groups at 8 weeks post-operation; H&E staining of: (f, i) BG-XLS, (g, j) BG-XLS/GelMA-DFO, (h, k) BG-XLS-BMP2 scaffolds at 8 weeks post-operation. *$P < 0.05$, **$P < 0.01$ (n = 3–4).

favorable for cells penetration and new tissue growth (Fig. 12(f–h)). Potent new bone formation was found in BG-XLS/GelMA-DFO and BG-XLS-BMP2 scaffolds, while only new bone-like tissues were observed on BG-XLS scaffolds. The quantitative data of HE staining was shown in Table 1. These *in vivo* data revealed that the incorporation of XLS and DFO onto BG scaffolds together promoted the endogenous bone formation without using exogenous osteoinductive factors. The incorporation of XLS not only increased the stiffness of BG scaffolds, but also

Table 1
New bone formation in BG-XLS, BG-XLS/GelMA-DFO and GF-XLS-BMP2 groups after 8 weeks of implantation.

	BG-XLS	BG-XLS/ GelMA-DFO	BG-XLS-BMP2
Scaffolds with new bone formation/total scaffolds	2/3	4/4	3/3
New bone area fraction (%)	10.06 ± 9.04	21.44 ± 4.60	34.24 ± 9.11

enhanced osteogenic differentiation of stem cells . The enhanced osteogenic abilities of XLS were mainly due to two reasons: firstly, the XLS can strongly binding with pro-osteoblastic factors, such as BMPs; secondly, the degradation products from XLS also had positive effects on the osteogenesis of stem cells [21,49,50]. Moreover, the elevated HIF-1α and VEGF expressions in ADSCs *in vitro* suggested the BG-XLS/GelMA-DFO scaffolds had the ability to promote angiogenesis likely through hypoxia mimicking agent activated HIF- 1α signaling pathway [16]. All these data indicated that the prepared nanoclay functionalized hypoxia-mimicking BG scaffold is a promising strategy to promote endogenous bone formation.

4. Conclusions

In this work, a nanoclay-decorated BG scaffold with osteoinductive and hypoxia mimicking properties was successful prepared via a combination of foam replication together with photo-crosslinking method. The incorporated amount of XLS was investigated based on the morphology, porosity and the mechanical property of BG-XLS scaffolds. DFO was physically blended with GelMA before immobilizing onto the BG-XLS scaffold for photo-crosslinking. Our results revealed that BG-XLS/GelMA-DFO had a sustained DFO release behavior for a period of 21 days and maintained the ability to increased HIF-1α and VEGF expressions in ADSCs. Moreover, our *in vitro* data also demonstrated BG-XLS/GelMA-DFO scaffold enhanced osteogenic differentiation of ADSCs compared to the BG scaffold. Our *in vivo* data further indicated that BG-XLS/GelMA-DFO scaffold significantly improved bone formation in a critical-sized SD rat calvaria defect model. Overall, we developed an innovative hypoxia mimicking bioglass-nanoclay scaffold with both osteogenic and angiogenic properties, and is a promising alternative for bone tissue engineering.

Credit author statement

Xiao Zheng contributes to the Methodology; Xiaorong Zhang and Yingting Wang contribute to the Project administration; Yangxi Liu contributes to Writing-review & editing; Yining Pan, Yijia Li and Man Ji contribute to the Data curation; Xueqin Zhao is responsible for paper editing; Shengbin Huang and Qingqing Yao are responsible for the ideas of the paper, designing the experimental route and writing the paper.

Acknowledgements

This work is supported by the Chinese National Natural Science Foundation of China (31600773) and Zhejiang Provincial Natural Science Foundation of China (LY18C100002).

References

[1] R. Marsell, T.A. Einhorn, The biology of fracture healing, Injury 42 (2010) 551–555.
[2] R. Dimitriou, E. Tsiridis, P.V. Giannoudis, Current concepts of molecular aspects of bone healing, Injury 36 (2005) 1392–1404.
[3] D.B. Burr, M.A. Gallant, Bone remodelling in osteoarthritis, Nat. Rev. Rheumatol. 8 (2012) 665–673.
[4] K. Schmidt-Bleek, B.J. Kwee, D.J. Mooney, G.N. Duda, Boon and bane of inflammation in bone tissue regeneration and its link with angiogenesis, Tissue Eng. B Rev. 21 (2015) 354–364.
[5] E. Gómez-Barrena, P. Rosset, D. Lozano, J. Stanovici, C. Ermthaller, F. Gerbhard, Bone fracture healing: cell therapy in delayed unions and nonunions, Bone 70 (2015) 93–101.
[6] Y. Leng, F. Yang, Q. Wang, Z. Li, B. Yuan, C. Peng, G. Ren, Z. Wang, Y. Cui, Y. Wang, L. Zhu, H. Liu, D. Wu, Materials-based therapy for bone nonunion, Mater. Des. 183 (2019) 108161.
[7] M. Torres-Torrillas, M. Rubio, E. Damia, B. Cuervo, A. del Romero, P. Peláez, D. Chicharro, L. Miguel, J.J. Sopena, Adipose-derived mesenchymal stem cell: a promising tool in the treatment of musculoskeletal diseases, Int. J. Mol. Sci. 20 (2019) 3105.
[8] K.D. Hankenson, M. Dishowitz, C. Gray, M. Schenker, Angiogenesis in bone regeneration, Injury 42 (2011) 556–561.
[9] M. Honda, R. Hariya, M. Matsumoto, M. Aizawa, Acceleration of osteogenesis via stimulation of angiogenesis by combination with scaffold and connective tissue growth favor, Materials 12 (2019) 2068.
[10] J. Filipowska, K.A. Tomaszewski, L. Niedzwiedzki, J. Walocha, T. Niedzwiedzki, The role of vasculature in bone development, regeneration and proper systemic functioning, Angiogenesis 20 (2017) 291–302.
[11] T. Matsumoto, S. Sato, Stimulating angiogenesis mitigates the unloading-induced reduction in osteogenesis in early-stage bone repair in rats, Phys. Rep. 3 (2015), e12335.
[12] J. Chen, L. Deng, C. Porter, G. Alexander, D. Patel, J. Vines, X.X. Zhang, D. Chasteen-Boyd, H.J. Sung, Y.P. Li, A. Javed, S. Gilbert, K. Cheon, H.W. Jun, Angiogenic and osteogenic synergy of human mesenchymal stem cells and human umbilical vein endothelial cells cocultured on a nanomatrix, Sci. Rep. 8 (2018) 15749.
[13] S. Hosseinpour, R. Fekrazad, P.R. Arany, Q.S. Ye, Molecular impacts of photobiomodulation on bone regeneration: a systematic review, Prog. Biophys. Mol. Biol. 149 (2019) 147–159.
[14] Z.P. Liu, X. Yin, Q.S. Ye, W.L. He, M.K. Ge, X.F. Zhou, J. Hu, S.J. Zou, Periodontal regeneration with stem cells-seeded collagen-hydroxyapatite scaffold, J. Biomater. Appl. 31 (2016) 121–131.
[15] H.X. Xie, Z.P. Gu, Y. He, J. Xu, C. Xu, L.J. Li, Q.S. Ye, Microenvironment construction of strontium–calcium-based biomaterials for bone tissue regeneration: the equilibrium effect of calcium to strontium, J. Mater. Chem. B 6 (2018) 2332–2339.
[16] Q. Yao, Y. Liu, J. Tao, K.M. Baumgarten, H. Sun, Hypoxia-mimicking nanofibrous scaffolds promote endogenous bone regeneration, ACS Appl. Mater. Interfaces 8 (2016) 32450–32459.
[17] E. Flume, J. Barberi, E. Verné, F. Baino, Bioactive glasses: from parent 45S5 composition to scaffold-assisted tissue-healing therapies, J. Funct. Biomater. 9 (2018) 24.
[18] M.N. Rahaman, D.E. Day, B.S. Bai, Q. Fu, S.B. Jung, L.F. Bonewald, A.P. Tomsia, Bioactive glass in tissue engineering, Acta Biomater. 7 (2011) 2355–2373.
[19] G.G. Niederauer, M.A. Slivka, N.C. Leatherbury, D.L. Korvick, H.H. Harroff Jr., W. C. Ehler, C.J. Dunn, K. Kieswetter, Evaluation of multiphase implants for repair of focal osteochondral defects in goats, Biomaterials 21 (2000) 2561–2574.
[20] Q. Yao, P. Nooeaid, R. Detsch, J.A. Roether, Y. Dong, Q.-M. Goudouri, D. W. Schubert, A.R. Boccaccini, Bioglass/chitosan–polycaprolactone bilayered composite scaffolds intended for osteochondral tissue engineering, J. Biomed. Mater. Res. A. 102A (2014) 4510–4518.
[21] A. Hoppe, N.S. Güldal, A.R. Boccaccini, A review of the biological response to ionic dissolution products from bioactive glass and glass-ceramics, Biomaterials 32 (2011) 2757–2774.
[22] B.A.E. Ben-Arfa, S. Neto, I.M.M. Salvado, R.C. Pullar, J.M.F. Ferreira, Robocasting of Cu^{2+} & La^{3+} doped sol-gel glass scaffolds with greatly enhanced mechanical properties: compressive strength up to 14 MPa, Acta Biomater. 87 (2019) 265–272.
[23] H.X. Xie, Z.P. Gu, C.S. Li, C. Franco, J.Y. Wang, L.J. Li, N. Meredith, Q.S. Ye, C. X. Wan, A novel bioceramic scaffold integrating silk fibroin in calcium polyphosphate for bone tissue-engineering, Ceram. Int. 42 (2016) 2386–2392.
[24] S. Heidari, T. Hooshmand, B.E. Yekta, A. Tarlani, N. Noshiri, M. Tahriri, Effect of addition of titanium on structural, mechanical and biological properties of 45S5 glass-ceramic, Ceram. Int. 44 (2018) 11682–11692.
[25] C. Xu, Y.X. Cao, C. Lei, Z.H. Li, T. Kumeria, A.K. Meka, J. Xu, J.Y. Liu, C. Yan, L. H. Luo, Polymer–mesoporous silica nanoparticle core–shell nanofibers as a dual-drug-delivery system for guided tissue regeneration, ACS Appl. Nano Mater 3 (2020) 1457–1467.
[26] Y.Y. Cao, P. Wu, C.D. Gao, P. Feng, T. Xiao, Y.W. Deng, C.J. Shuai, S.P. Peng, A 45S5 bioactive glass scaffold reinforced with ZnO and MgO, J. Biomater. Tissue Eng. 6 (2016) 98–106.
[27] J.R. Xavier, T. Thakur, P. Desai, M.K. Jaiswal, N. Sears, E. Cosagriff-Hernandez, R. Kaunas, A.K. Gaharwar, Bioactive nanoengineered hydrogels for bone tissue engineering: a growth-factor-free approach, ACS Nano 9 (2015) 3109–3118.
[28] L. Han, X. Lu, K. Liu, K. Wang, L. Fang, L.T. Weng, H. Zhang, Y. Tang, F. Ren, C. Zhao, G. Sun, R. Liang, Z. Li, Mussel-inspired adhesive and tough hydrogel based on nanoclay confined dopamine polymerization, ACS Nano 11 (2017) 2561–2574.
[29] P. Shi, Y.-H. Kim, M. Mousa, R.R. Sanchez, R.O.C. Oreffo, J.I. Dawson, Self-assembling nanoclay diffusion gels for bioactive osteogenic microenvironments, Adv. Healthcare Mater 7 (2018) 1800331.
[30] A.K. Gaharwar, S.M. Mihaila, A. Swami, A. Patel, S. Sant, R.L. Reis, A.P. Marques, M.E. Gomes, A. Khademhosseini, Bioactive silicate nanoplatelets for osteogenic differentiation of human mesenchymal stem cells, Adv. Mater. 25 (2013) 3329–3336.

[31] T. Cebe, N. Ahuja, F. Monte, K. Awad, K. Vyavhare, P. Aswath, J. Huang, M. Brotto, V. Varanasi, Novel 3D-printed methacrylated chitosan-laponite nanosilicate composite scaffolds enhance cell growth and biomineral formation in MC3T3 pre-osteoblasts, J. Mater. Res. 35 (2020) 58–75.
[32] G. Cidonio, C.R. Alcala-Orozco, K.S. Lim, M. Glinka, I. Mutreja, Y.-H. Kim, J. I. Dawson, T.B.F. Woodfield, R.O.C. Oreffo, Osteogenic and angiogenic tissue formation in high fidelity nanocomposite laponite-gelatin bioinks, Biofabrication 11 (2019), 035027.
[33] C. Wang, S. Wang, K. Li, Y. Ju, J. Li, Y. Zhang, J. Li, X. Liu, X. Shi, Q. Zhao, Preparation of Laponite bioceramics for potential bone tissue engineering applications, PloS One 9 (2014), e99585.
[34] Q. Yao, W. Li, S. Yu, L. Ma, D. Jin, A.R. Boccaccini, Y. Liu, Multifunctional chitosan/polyvinyl pyrrolidone/45S5 Bioglass scaffolds for MC3T3-E1 cell stimulation and drug release, Mater. Sci. Eng. C 56 (2015) 473–480.
[35] T. Kokubo, K. Hata, T. Nakamura, T. Yamamura, Apatite formation on ceramics, metals, and polymers induced by a CaO–SiO2-based glass in simulated body fluid, in: W. Bonfield, G.W. Hastings, K.E. Tanner (Eds.), Bioceramics, vol. 4, Guildford, Butterworth-Heinemann, London, 1991, pp. 113–120.
[36] Q. Yao, J.G.L. Cosme, T. Xu, J.M. Miszuk, P.H.S. Picciani, H. Fong, H. Sun, Three dimensional electrospun PCL/PLA blend nanofibrous scaffolds with significantly improved stem cells osteogenic differentiation and cranial bone formation, Biomaterials 115 (2017) 115–127.
[37] G. Akay, M.A. Birch, M.A. Bokhari, Microcellular polyHIPE polymer supports osteoblast growth and bone formation in vitro, Biomaterials 25 (2004) 3991–4000.
[38] A. Artel, H. Mehdizadeh, Y.C. Chiu, E.M. Brey, A. Cinar, An agent-based model for the investigation of neovascularization within porous scaffolds 17 (2011) 2133–2141.
[40] L.L. Hench, J.R. Jones, Bioactive glass: frontiers and challenges, Front. Bioeng. Biotechnol. 3 (2015) 194.
[42] L. Millucci, M. Minetti, M. Orlandini, D. Braconi, M.L. Schiavone, S. Galderisi, B. Marzocchi, O. Spiga, R. Rappuoli, A. Spreafico, Beer promotes differentiation and mineralization of human osteoblastic cells: role of silicon, J. Fuct. Foods 54 (2019) 109–118.
[43] M. Julien, S. Khoshniat, A. Lacreusette, M. Gatius, A. Bozec, E.F. Wagner, Y. Wittrant, M. Masson, P. Weiss, L. Beck, D. Magne, J. Guicheux, Phosphate-dependent regulation of MGP in osteoblasts: role of ERK1/2 and Fra-1, J. Bone Miner. Res. 24 (2009) 1856e68.
[45] F. Zhang, C.J. Phiel, L. Spece, N. Gurvich, P.S. Klein, Inhibitory phosphorylation of glycogen synthase kinase-3 (GSK-3) in response to lithium- evidence for autoregulation of GSK-3, J. Biol. Chem. 278 (2003) 33067–33077.
[46] Q. Yao, Y. Liu, B. Selvaratnam, R.T. Koodali, H. Sun, Mesoporous silicate nanoparticles/3D nanofibrous scaffold-mediated dual-drug delivery for bone tissue engineering, J. Contr. Release 279 (2018) 69–78.
[47] A.K. Gaharwar, S.M. Mihaila, A. Swami, A. Patel, S. Sant, R.L. Reis, A.P. Marques, M.E. Gomes, A. Khademhosseini, Bioactive silicate nanoplatelets for osteogenic differentiation of human mesenchymal stem cells, Adv. Mater. 25 (2013) 3329–3336.
[49] Q. Yao, K.E. Fuglsby, X. Zheng, H. Sun, Nanoclay-functionalized 3D nanofibrous scaffolds promote bone regeneration, J. Mater. Chem. B 17 (2020) 3842–3851.
[50] C. Aguzzi, P. Cerezo, C. Viseras, C. Caramella, Use of clays as drug delivery systems: possibilities and limitations, Appl. Clay Sci. 36 (2007) 22–36.